ELSEVIER

Catalysis Today 48 (1999) 161–174

CATALYSIS TODAY

Modeling of acetophenone hydrogenation over a Rh/C catalyst in a slurry airlift reactor

I. Bergault[a,*], C. Joly-Vuillemin[b], P. Fouilloux[b], H. Delmas[a]

[a]*LGC – Laboratoire de Génie Chimique, Toulouse, France*
[b]*LGPC – CPE Lyon, Laboratoire du Génie des Procédés Catalytiques, Villeurbanne, France*

Abstract

The hydrogenation of acetophenone in a slurry airlift reactor was conducted over a wide range of operating conditions. An important deactivation of the catalyst was experimentally observed and an empirical deactivation law was optimized. The deactivation rate constant increases with the inlet concentration and gas flow rate and decreases with the catalyst loading. The product selectivity measured in the slurry airlift reactor did not fit well with the computed one. The computation was performed using the results of the kinetic and hydrodynamic studies. A sensitivity analysis pointed out that the mass transfer is not limited. To perform a good fit with the experiments it was necessary to change some rate constants. This readjustment was justified by the difference in catalyst pretreatment between the continuous and the semi-batch reactor where significant catalyst pretreatment effects were shown. © 1999 Elsevier Science B.V. All rights reserved.

Keywords: Multiphase reactors; Heterogeneous catalysis; Airlift; Deactivation

1. Introduction

Slurry airlift reactors are extensively used in chemical industrial processes such as hydrogenation and oxidation. They provide good heat and mass transfer efficiencies for a low power requirement. This is their great advantage. However, the performances of such catalytic multiphase reactors are difficult to predict, and more especially when the reaction scheme is complex [1–3]. On one hand, it requires hydrodynamics, mass and heat transfer knowledge coupled to complex kinetic models. All these topics need to be studied separately. On the other hand, the knowledge of some catalytic phenomena such as deactivation or catalyst pretreatment effects should also be taken into account.

In the present work, performances of a slurry airlift reactor were studied on an industrially relevant case: hydrogenation of acetophenone. This reaction was chosen as an example of a complex reaction with multiple steps involved The reported results [4–11] show clearly the strong dependence of the reaction scheme towards the catalyst nature and operating conditions. Most of the kinetic studies reported in the literature concern the selective hydrogenation of acetophenone into phenyl 1-ethanol followed by the hydrogenolysis in ethylbenzene. Power law kinetics are often proposed to represent the data [6,7,12–15] and only a few models based on the more realistic Langmuir–Hinshelwood hypothesis are available [10,17,18]. The reaction at the catalyst surface is

*Corresponding author.

0920-5861/99/$ – see front matter © 1999 Elsevier Science B.V. All rights reserved.
PII: S0920-5861(98)00370-8

always considered to be the rate limiting step. Some authors propose a competitive adsorption of the species but they are not able to choose between a dissociative or non-dissociative adsorption of hydrogen. Either they performed their experiments at a constant hydrogen pressure [16], or the agreement between the experimental results and the computed values obtained with the dissociative and non-dissociative models is not significantly different [10,17].

First of all, the intrinsic kinetics of acetophenone hydrogenation were studied in a semi-batch reactor [19]. The reaction was carried out using acetophenone (Aldrich, 99% mini), cyclohexane (RP Normapur Prolabo 99.5% mini) as a solvent and in the presence of a Rh catalyst supported on coconut shell activated carbon (Degussa, 3 wt% Rh/C, G181 XKB/D). Crushed catalyst particles of an average diameter ($d_p = 17 \times 10^{-6}$ m) were used. In each experiment, the catalyst was first pretreated in solvent under hydrogen pressure (18×10^5 Pa) during 1 h at 368 K. From gas chromatography analysis, several hydrogenation products of the aromatic ring and/or of the ketone function were identified. Hydrogenations of pure intermediates, like phenyl 1-ethanol (PE) or methylcyclohexylketone (MCC), were also performed and the analysis of the results led to the complex reaction scheme presented in Fig. 1. Kinetics of the reaction were studied using constant hydrogen pressures varying from 5×10^5 to 40×10^5 Pa, temperatures from 333 to 373 K and acetophenone initial concentrations from 0.118 to 1.14 kmol m^3. Several Langmuir–Hinshelwood kinetic models were developed depending on the rate limiting step. Discrimination and parameter optimization were performed using a commercial software (MKF, Cheminform, Saint Petersburg, Russia). The model assuming a non-dissociative adsorption of hydrogen and non-competitive adsorption between organic species and hydrogen provided the best fit of the experimental data, over a wide range of operating conditions [19]. Rate equations and kinetic parameter values are summarized in Table 1.

The present work deals with the slurry airlift reactor study. In order to develop a complete model describing the continuous reactor performances, hydrodynamics of the airlift reactor were first investigated and hydrogenations were carried out over a wide range of operating conditions. Gas–liquid mass transfer limitations, catalyst deactivation as well as catalyst pretreatment effects were studied in detail and discussed.

2. Experimental

The schematic of the slurry airlift reactor is presented in Fig. 2. Hydrodynamics were investigated in

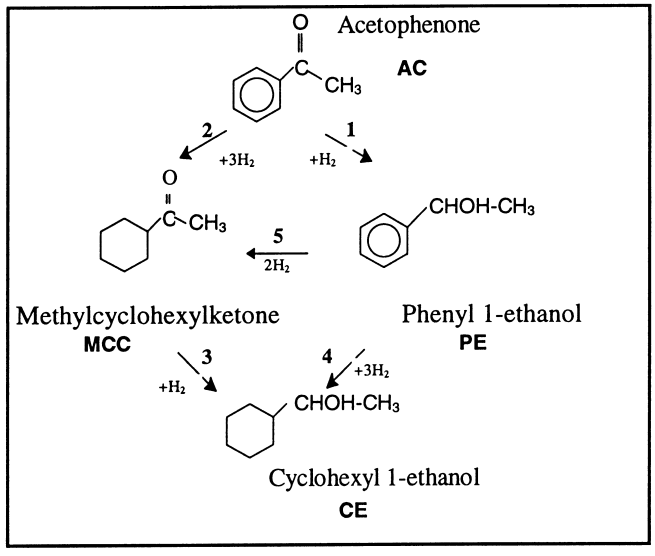

Fig. 1. Reaction scheme of acetophenone hydrogenation on Rh/C catalyst.

Table 1
Kinetic rate expressions and parameters

$r_1 = k_1 Q_{AC}[AC]N/D$; $r_2 = k_2 Q_{AC}[AC]N/D$; $r_3 = k_3 Q_{MCC}[MCC]N/D$;

$r_4 = k_4[PE]N/D$; $r_5 = k_5[PE]N/D$,

with $k_i = k_i^o \exp(-E_i/RT)$, $K_{H_2} = K_{H_2}^o \exp(-\Delta H_H/RT)$, $N = K_{H_2} P_{H_2} = K_{H_2} He[H_2]$,
$D = (1/K_{PE} + Q_{AC}[AC] + [PE] + Q_{MCC}[MCC] + Q_{CE}[CE])(1 + K_{H_2} He[H_2])$

$\ln k_1^o$	26.98	E_1 (kJ mol^{-1})	79.65
$\ln k_2^o$	25.41	E_2 (kJ mol^{-1})	80.79
$\ln k_3^o$	20.16	E_3 (kJ mol^{-1})	69.47
$\ln k_4^o$	27.77	E_4 (kJ mol^{-1})	84.62
$\ln k_5^o$	30.79	E_5 (kJ mol^{-1})	100.26
$K_{H_2}^o$ (MPa^{-1})	9.97×10^{-9}	ΔH_H (kJ mol^{-1})	−49.51
Q_{MCC}	0.63	Q_{AC}	1.68
Q_{CE}	5.7×10^{-2}	K_{PE} (m^3 kmol^{-1})	100

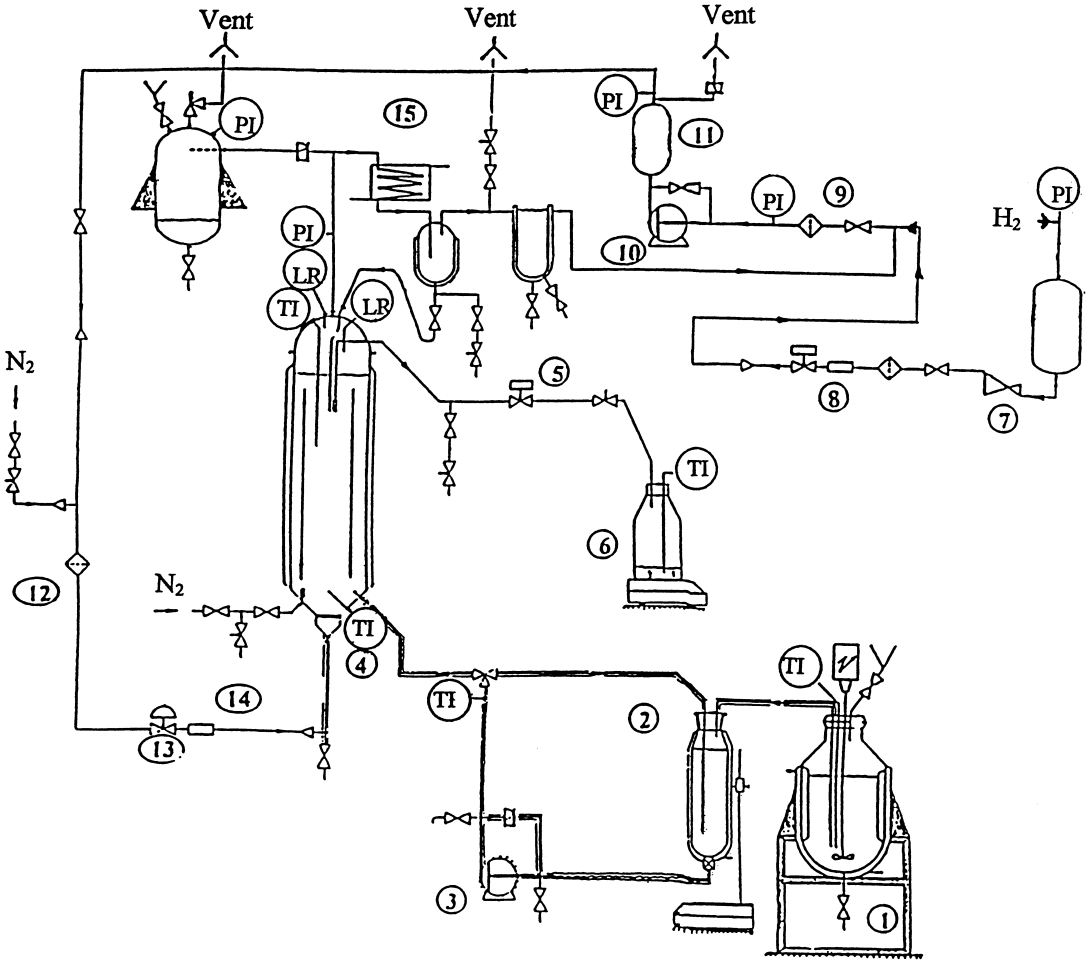

Fig. 2. Schematic set-up of the slurry airlift reactor.

exactly the same scale transparent bubble column with draught tube.

The reactor consists of a stainless steel tube of 57.1×10^{-3} m inner diameter and 1 m length. The draught tube is 75×10^{-2} m long and of 30.5×10^{-3} inner diameter. The reactor was operated continuously with respect to both gas and liquid phases. The temperature of the column was controlled by a jacket. Liquid and gas were fed and withdrawn through porous plates (pore diameter=15×10^{-6} m) which maintained the catalyst confined. The level of the gas–liquid–solid mixture in the column was controlled by ultrasonic probes coupled to the outlet valve. Hydrogen which has not reacted was fully recycled and the gas flow rate was regulated. For each experiment, the catalyst (Rh/C 3 wt%, $d_p=17\times10^{-6}$ m) was first pretreated in cyclohexane, under hydrogen flow ($P_{H_2} = 18 \times 10^5$ Pa, $T=$ 368 K, 1 h). The reactor was set to the desired temperature and pressure and acetophenone solution introduced at the bottom of the column (defining the initial time). The pressure and flow rate controllers provided the amount of hydrogen consumed by the reaction. Liquid samples without solid particles were withdrawn at regular intervals of time from the bottom and from the top of the reactor and analyzed by gas chromatography. Experiments were performed at $T=$ 353K and $P_{H_2} = 20 \times 10^5$ Pa and the following range of conditions were investigated: inlet concentration (0.2–0.475) kmol m^{-3}, catalyst loading (3×10^{-3}–10×10^{-3}) kg, gas velocity (3.7×10^{-3}–2×10^{-2}) m s^{-1}.

3. Results and discussion

3.1. Hydrodynamics

The volumetric hydrogen mass transfer coefficient was measured by absorption of oxygen into cyclohexane, as the density of air at atmospheric pressure and ambient temperature is close to the one of hydrogen at $P_{H_2} = 2$ MPa and $T=353$ K. Based on the theory of surface renewal proposed by Hibgie and Danckwerts [20,21], values of k_La for H_2 were deduced from those for O_2 by multiplying $(k_La)_{O_2}$ by the ratio: $[D_{H_2}/D_{O_2}]^{1/2}$. Molecular diffusivities were calculated by the correlation of Wilke and Chang [22]. The gas hold-up was estimated as a function of gas velocity by comparison between the aerated and non-aerated volumes of the solution. Effects of catalyst loading were investigated and Figs. 3 and 4 show the evolution of the gas hold-up ϵ_G and the volumetric hydrogen mass transfer coefficient k_La over the range of gas velocities u_G used in the airlift reactor, for several catalyst concentrations ($C_S=m_{cata}/m_{solvent}$). The observed trends versus gas velocity are those commonly encountered in [23–27]. Slightly lower values of ϵ_G and k_La were obtained at identical gas velocity, in presence of solid particles. This result could be explained by an increase of gas coalescence due to the presence of fine particles, leading to slightly larger bubbles.

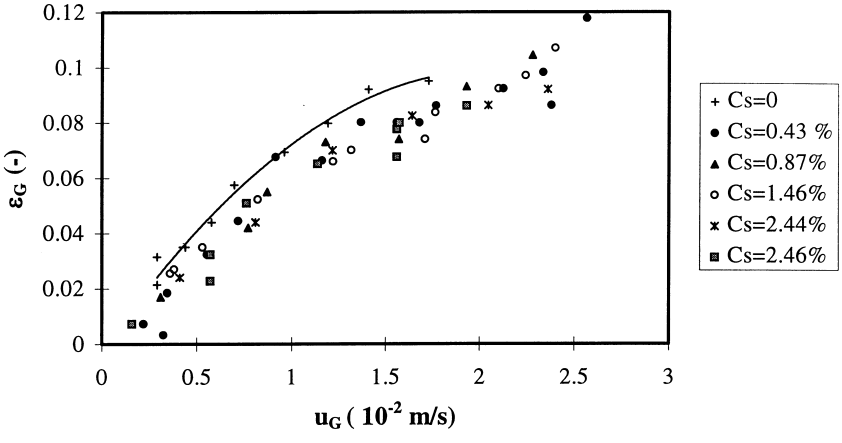

Fig. 3. ϵ_G versus gas velocity.

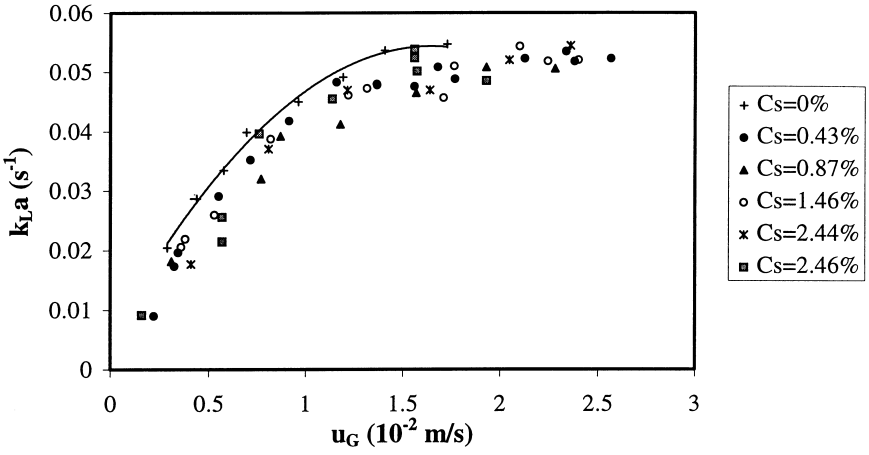

Fig. 4. $(k_La)_{H_2}$ versus gas velocity.

3.2. *Hydrogenations in the continuous airlift reactor*

For each experiment, hydrogen consumption (instantaneous hydrogen flow rate consumed) as well as the outlet concentration profiles for each species (AC, PE, MCC, CE) were plotted, as a function of time. As shown in the typical curve plotted in Fig. 5, hydrogen consumption decreases with time for each experiment. This result indicates some deactivation of the catalyst which might depend on the operating conditions. Looking at the concentration profiles in Fig. 6, the same conclusion can be drawn. Acetophenone concentration keeps on increasing with time even after reaching the hydrodynamic steady state, meaning that conversion decreases instead of being stable.

In addition to deactivation, classical trends were observed: hydrogen consumption and conversion increased with increasing catalyst loading and acetophenone conversion decreased with increasing the inlet acetophenone flow rate. Gas velocity was found to slightly affect conversion: at equal time of reaction, hydrogen consumption was slightly lower at high gas flow rate. These observed effects being the result of combined deactivation and operating parameters effects, a reactor model was developed and a sensitivity analysis of the parameters performed in order to evaluate the contribution of each phenomenon.

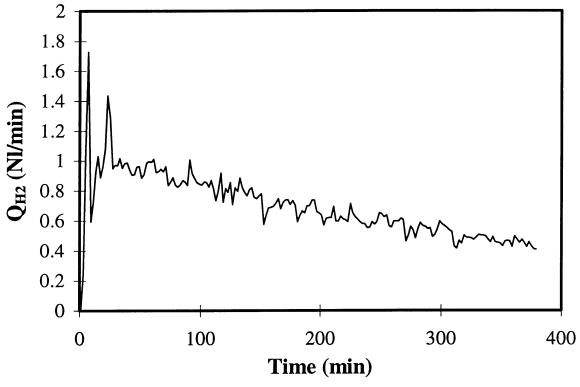

Fig. 5. Hydrogen consumption versus time. $P_{H_2} = 2$ MPa, T=353 K, $C^{o}_{AC} = 0.475$ kmol m^{-3}, m_{cata}=5×10^{-3} kg, Q_L=4.72×10^{-7} m^3 s^{-1}, u_G=1.5×10^{-2} m s^{-1}.

4. Modeling of the airlift reactor

4.1. *Assumptions*

1. Based on the instantaneous comparison of concentrations between the bottom and the top of the column, the liquid phase was considered as perfectly mixed.
2. From experiments performed in the semi-batch reactor, it was proved that neither internal diffusion nor liquid–solid mass transfer was limiting.
3. The rate equations and kinetic parameter values given in Table 1, as well as the experimental values of the hydrodynamic parameters given in Figs. 3 and 4, were used.

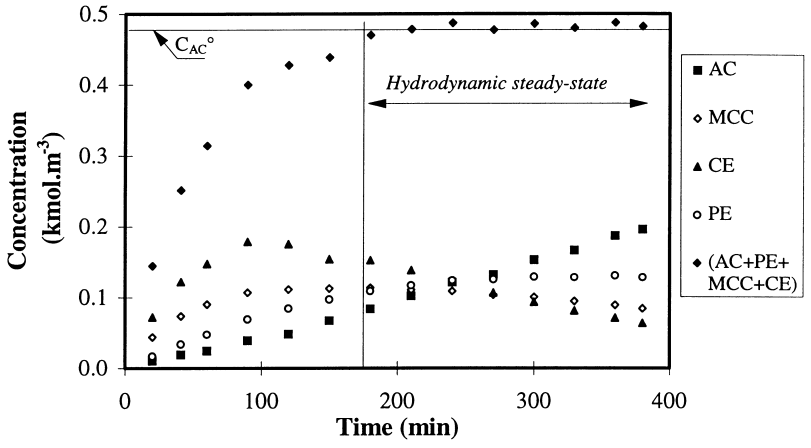

Fig. 6. Concentration profiles versus time. $P_{H_2} = 2\,MPa$, T=353 K, $C^{o}_{AC} = 0.475\,kmol\,m^{-3}$, m_{cata}=5×10^{-3} kg, Q_L=$4.72\times10^{-7}\,m^3\,s^{-1}$, u_G=$1.5\times10^{-2}\,m\,s^{-1}$.

4. A deactivation law detailed below was introduced in the model in order to represent the experimental results.

4.2. Choice of the deactivation rate equation

Deactivation of catalysts is quite common in chemical and petrochemical industrial processes, but the way to model this complex phenomenon is not yet well established. Based on the analysis of Levenspiel [28] and Froment and Bischoff [29], different types and mechanisms of deactivation can be described. The first one is the sintering of the catalyst which generally occurs at high temperature, and consists of a physical change in the catalyst structure. The second one, often encountered in petrochemical industry, is the coking of the catalyst which consists of deposit of a carbonaceous residue, resulting in pore blockage. The last usual cause of deactivation and the most probable here is the catalyst poisoning by irreversible chemisorption of an impurity.

Depending on the knowledge of deactivation mechanisms, several kinetic approaches can be proposed. The first approach consists of a phenomenological description of deactivation. As soon as the poison (the impurity which is likely to irreversibly adsorb or a precursor of this impurity) can be identified and quantified, it is possible to describe the presumed mechanisms of deactivation and to express their kinetics as a function of the poison concentration. However, when the measurement of this concentration is not possible, empirical equations have to be used. As an example, the fraction of deactivated sites θ_{des} can be introduced in the model and expressed as a function of observable parameters (like coke content, reactant flow rate per weight of catalyst, time of reaction, etc.).

In our case, several analyses (gas chromatography coupled to mass spectrometry, sulfur contents, liquid impurity contents) of all the reagents were performed in order to identify the possible poisons of the catalyst but the causes and mechanisms of deactivation remained unexplained and only empirical equations could be tested. First of all, four types of deactivation rates were discriminated using the experimental data of hydrogen consumption versus time (see Table 2).

A and k_d are deactivation parameters depending on operating conditions so computed for each experiment.

Typical results compared in Fig. 7 with various optimized deactivation rates show that the best fit is obtained for the first-order type law. Zero order would have required a linear decrease of hydrogen consumption with time, and second- and third-order type laws,

Table 2

Order of the deactivation law	0	1	2	3
Q_{H_2}	$A-k_d t$	$A\exp(-k_d t)$	$A/(1+k_d t)$	$A(1+k_d t)^{-0.5}$
dQ_{H_2}/dt	$-k_d$	$-k_d Q_{H_2}$	$-k_d Q^2_{H_2}$	$-k_d Q^3_{H_2}$

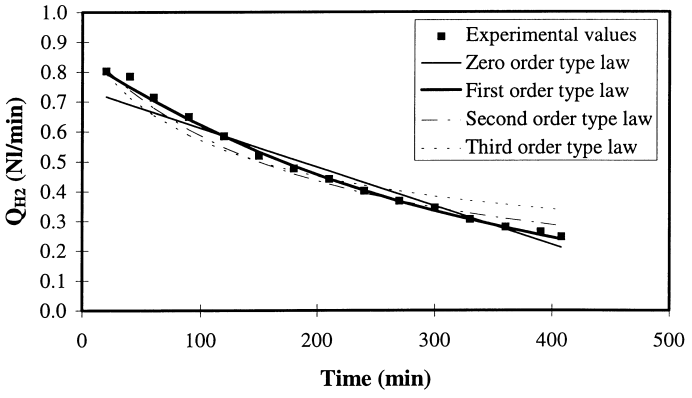

Zero order type law: Q_{H2}(Nl/min)=A-k_dt A(Nl/min) = 0.7416; $k_d = 2.17*10^{-5}\ s^{-1}$	Second order type law: Q_{H2}(Nl/min)=A/ (1+ k_dt) A(Nl/min) = 0.895 ; $k_d = 8.83*10^{-5}\ s^{-1}$
First order type law: Q_{H2}(Nl/min)=A*exp(-k_d t) A(Nl/min) = 0.8475; $k_d = 5.17*10^{-5}\ s^{-1}$	Third order type law: Q_{H2}(Nl/min)=A(1+K_d t)$^{-0,5}$ A(Nl/min) = 0.904 ; $k_d = 2.53*10^{-4}\ s^{-1}$

with t expressed in seconds.

Fig. 7. (1) Zero-order type law: Q_{H_2} (Nl/min) $= A - k_d t$, A (Nl/min)=0.7416, k_d=2.17×10^{-5} s^{-1}; (2) first-order type law: Q_{H_2} (Nl/min) $= A \times \exp(-k_d t)$, A (Nl/min)=0.8475, k_d=5.17×10^{-5} s^{-1}; (3) second-order type law: Q_{H_2}(Nl/min) $= A/(1 + k_d t)$, A (Nl/min)=0.895, k_d=8.83×10^{-5} s^{-1}; (4) third-order type law: Q_{H_2} (Nl/min) $= A(1 + K_d t)^{-0.5}$, A (Nl/min)=0.904, k_d=2.53×10^{-4} s^{-1}. Experimental hydrogen consumption versus time represented by four empirical deactivation laws. $P_{H_2} = 2$ MPa, T=353 K, $C^o_{AC} = 0.475$ kmol m^{-3} m_{cata}=3×10^{-3} kg, Q_L=4.72×10^{-7} m^3 s^{-1}, u_G=1.5×10^{-2} m s^{-1}.

a faster deactivation of the catalyst at the beginning. A first-order deactivation rate was then chosen and introduced in the airlift reactor model.

4.3. Mass balance equations of the airlift reactor

θ_{des} being the fraction of the deactivated sites at the reaction time t, $(1-\theta_{des})$ is the fraction of remaining active sites. Every reaction rate is proportional to the fraction of active sites and can be expressed as $r_i = r_i^o \times (1 - \theta_{des})$ where r_i^o (i=1–5) is the initial rate without deactivation given in Table 1.

Introducing in the model a first-order deactivation rate based on the fraction of remaining active sites leads to the mass balance equations for the airlift slurry reactor, presented in Table 3.

Table 3
Mass balance equations for the airlift slurry reactor

$$\frac{dC_{AC}}{dt} = \frac{Q_L}{V_r(1-\epsilon_G)}(C^o_{AC} - C_{AC}) - (r^o_1 + r^o_2)(1-\vartheta_{des})\frac{m_{cata}}{V_r(1-\epsilon_G)}$$

$$\frac{dC_{PE}}{dt} = (r^o_1 - r^o_4 - r^o_5)(1-\vartheta_{des})\frac{m_{cata}}{V_r(1-\epsilon_G)} - \frac{Q_L}{V_r(1-\epsilon_G)}C_{PE}$$

$$\frac{dC_{MCC}}{dt} = (r^o_2 + r^o_5 - r^o_3(1-\vartheta_{des})\frac{m_{cata}}{V_r(1-\epsilon_G)} - \frac{Q_L}{V_r(1-\epsilon_G)}C_{MCC}$$

$$\frac{dC_{CE}}{dt} = (r^o_3 + r^o_4)(1-\vartheta_{des})\frac{m_{cata}}{V_r(1-\epsilon_G)} - \frac{Q_L}{V_r(1-\epsilon_G)}C_{CE}$$

$$\frac{dC_{H_{2,1}}}{dt} = k_L a(C^*_{H_2} - C_{H_{2,1}}) - \frac{Q_L}{V_r(1-\epsilon_G)}C_{H_{2,1}} - \frac{m_{cata}}{V_r(1-\epsilon_G)}(r^o_1 + 3r^o_2 + r^o_3 + 3r^o_4 + 2r^o_5)(1-\vartheta_{des})$$

$$\frac{d\vartheta_{des}}{dt} = k_d(1-\vartheta_{des})$$

Initial conditions: t=0: C_{AC}=C_{PE}=C_{MCC}=C_{CE}=0; $C_{H_2} = C^*_{H_2}$; θ_{des}=0.

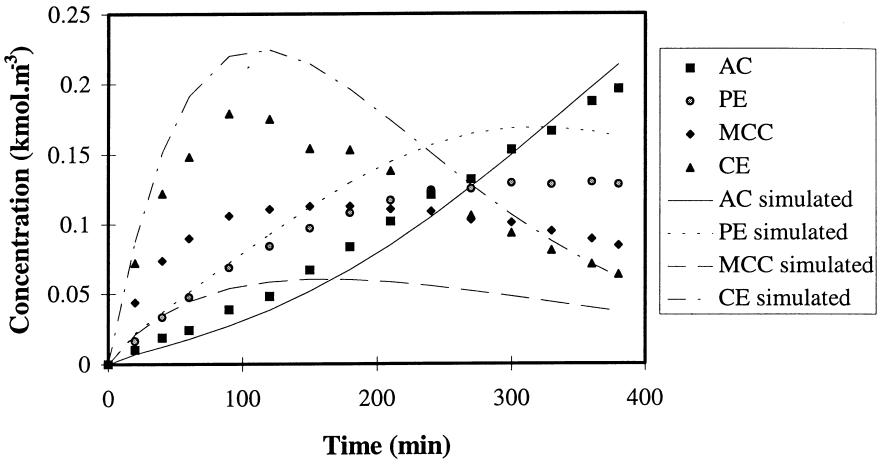

Fig. 8. Experimental and simulated concentration profiles versus time. First-order type deactivation law: k_d=9.63×10^{-5} s^{-1}. P_{H_2} = 2 MPa, T=353 K, C^o_{AC} = 0.475 kmol m^{-3}, m_{cata}=5×10^{-3} kg, Q_L=4.72×10^{-7} m^3 s^{-1}, u_G=1.5×10^{-2} m s^{-1}.

4.4. Sensitivity analysis

From the concentration profiles of liquid phase species at the outlet of the reactor, the deactivation parameter k_d was then optimized for each experiment. k_d values obtained were of the same order of magnitude when compared to the values estimated from the curves representing hydrogen consumption versus time (3×10^{-5} s$^{-1}\leq k_d\leq 1.2\times10^{-4}$ s^{-1}). As shown in Fig. 8, the simulated curves follow a similar trend to the experimental ones but selectivity is poorly predicted: at the beginning of each reaction run, methylcyclohexylketone is formed in higher quantities and cyclohexylethanol in lower quantities than those predicted by the model. This indicates that the proposed model including a first-order deactivation is able to represent the global hydrogenation process but not the selectivity. In order to clarify this problem, a sensitivity analysis of each parameter on the predictions was performed.

4.4.1. Effect of k_d

It is obvious that k_d is a highly sensitive parameter of the model, directly affecting the activity of the reaction. However, it is important to note that the same deactivation law was chosen for the five steps of the reaction scheme so a change in k_d value cannot, in any case, affect the predicted selectivity. For this purpose, a different deactivation law for each reaction should have been introduced in the model, which would have multiplied the number of parameters and the difficulty to estimate them with a good precision.

4.4.2. Effect of k_La

Since each reaction follows the same dependence toward hydrogen concentration in the liquid phase (see kinetic laws in Table 1), the gas–liquid mass transfer affects identically each reaction rate. Then, k_La value cannot affect the predicted selectivity. Even though the influence of gas–liquid mass transfer on the performances of the airlift reactor was estimated by varying the values of k_La from 0.1 to 5 times the value given by the hydrodynamic study. Simulation results were hardly not affected by the changes in k_La values, indicating that gas–liquid mass transfer was not limiting.

4.4.3. Effect of the kinetic parameters

They appear to be the only parameters of the model able to improve the representation of the experimental results. The analysis of their sensitivity was performed using the same commercial software (MKF, Cheminform, Saint Petersbourg, Russia) as for the kinetic study. This software uses an iterative method based on the linearization of the model equations and tries to minimize the value of the following optimization criterion: $\text{criterion}=\sum_i (Y_i^c - Y_i^{exp})^2/(\text{error}\times Y_i^{max})^2$.

A sensitivity analysis was performed on each experiment, optimizing independently each kinetic

Table 4
Sensitivity analysis of each kinetic parameter

	Initial value (issued from batch kinetics)	Optimized value	Initial value of the optimization criterion	Optimization criterion value after reoptimization of k_i
$\ln k_1^o$	26.98	26.49	2693	1657
$\ln k_2^o$	25.41	26.48	2693	244
$\ln k_3^o$	20.16	<10	2693	2691
$\ln k_4^o$	27.77	27.69	2693	2667
$\ln k_5^o$	30.79	32.69	2693	237
Q_{AC}	1.68	1.77	2693	2687
Q_{MCC}	0.63	0.97	2693	2640
Q_{CE}	5.77×10^{-2}	0.16	2693	2627
K_{PE} (kmol m^{-3})	100	37.4	2693	2614

parameter. For this purpose, all the other parameters (kinetic constants, k_La, k_d) were kept to their standard value. As an example, Table 4 shows the results obtained on one representative experiment, indicating first a strong influence of k_2^o and k_5^o and a quite important sensitivity of the model to k_1^o. These results are consistent with the previously observed facts that the rate of formation of MCC was underestimated by the model and the rate of formation of PE was overestimated. On the opposite, the model is not sensitive to k_3^o since the criterion remains nearly constant whatever the k_3^o value is. In fact, even if MCC concentration profile is directly related to k_3^o, r_3 is always extremely low compared to r_2 and r_5. The final value of the criterion is also not much affected by k_4^o, adsorption constant ratios and K_{PE} values. So, as a conclusion, it is possible to improve the fitting to our experimental data by accelerating the rate of formation of MCC so by increasing k_2^o and/or k_5^o, and diminishing the rate of formation of PE that is to say diminishing k_1^o.

4.5. Final optimization results

In a first step, the optimization of two of the three sensitive parameters k_1^o, k_2^o and k_5^o was good enough to fit selectivity of both MCC and PE. An iterative method was used to perform an optimization of the values of k_1^o and k_2^o on the whole set of experimental data from the airlift reactor (eight experiments):

- First of all, the k_d values were fixed to those previously computed and k_1^o and k_2^o were then optimized on the whole experimental data (eight experiments).
- The new optimized values of k_1^o and k_2^o were then fixed and each k_d optimized in turn.

This iterative process was then repeated until the value of the optimization criterion reached its minimum. Table 5 summarizes the final parameter values of the airlift reactor model. They provide a good fit with all the experimental data over the studied range of operating conditions. The maximum deviation is of 20% between the simulated and experimental profiles. Figs. 9 and 10 show the fits obtained in the best and in the worse case.

As a conclusion, the airlift reactor model initially proposed, including a first-order deactivation type law, provides a satisfying representation of the experimental data, after readjustment of two kinetic rate constants and optimization of the deactivation parameter on each experiment.

5. Discussion

The first point to discuss is the reason why some kinetic parameters issued from the kinetic study in semi-batch reactor were not able to describe selectivities in airlift reactor.

The first possible reason is that the kinetic parameters were optimized without accounting for catalyst deactivation. In order to estimate the influence of deactivation on kinetic results in semi-batch reactor, a first-order deactivation rate was introduced in the kinetic model. First of all, when optimizing simulta-

Table 5
Parameters values of the airlift reactor model

Kinetic parameters common to all the experiments							
$\ln k_1^o$	26.98[a]	E_1 (kJ mol^{-1})	79.65	$\ln k_5^o$	30.79	E_5 (kJ mol^{-1})	100.26	$\ln k_2^o$
25.41[a]	E_2 (kJ mol^{-1})	80.79	$K_{H_2}^o$ (MPa^{-1})	9.97×10^{-9}	ΔH_{H} (kJ mol^{-1})	−49.51	$\ln k_3^o$	20.16
E_3 (kJ mol^{-1})	69.47	Q_{MCC}	0.63	Q_{AC}	1.68	$\ln k_4^o$	27.77	E_4 (kJ mol^{-1})
84.62	Q_{CE}	5.7×10^{-2}	K_{PE} (m^3 kmol^{-1})	100				

Gas–liquid mass transfer coefficients and deactivation constants

Run	P_{H_2} (MPa)	T (K)	C_{AC}^o (kmol m^{-3})	m_{cata} (kg)	Q_L (m^3 s^{-1})	u_G (m s^{-1})	k_La (s^{-1})	k_d (s^{-1})[a]
9	2	353	0.475	5×10^{-3}	4.72×10^{-7}	1.5×10^{-2}	4.75×10^{-2}	8.82×10^{-5}
10	2	353	0.475	5×10^{-3}	4.72×10^{-7}	1.5×10^{-2}	4.75×10^{-2}	8.22×10^{-5}
8	2	353	0.475	5×10^{-3}	4.72×10^{-7}	3.7×10^{-3}	2.73×10^{-2}	7.18×10^{-5}
6	2	353	0.475	5×10^{-3}	4.72×10^{-7}	2.04×10^{-2}	5.04×10^{-2}	1.13×10^{-4}
12	2	353	0.2	5×10^{-3}	4.72×10^{-7}	1.5×10^{-2}	4.75×10^{-2}	5.61×10^{-5}
11	2	353	0.475	10×10^{-3}	4.72×10^{-7}	1.5×10^{-2}	4.75×10^{-2}	3.74×10^{-5}
13	2	353	0.475	3×10^{-3}	4.72×10^{-7}	1.5×10^{-2}	4.75×10^{-2}	9.61×10^{-5}

[a] Indicates the reoptimized parameters.
k_La values are given by the hydrodynamic study, and the others by the kinetic study.

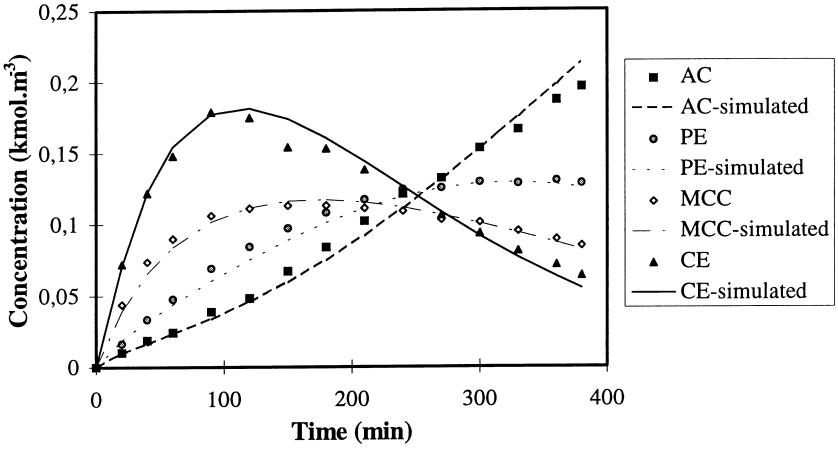

Fig. 9. Experimental and simulated concentration profiles versus time. $P_{H_2}=2$ MPa, T=353 K, $C_{AC}^o=0.475$ kmol m^{-3}, $m_{cata}=5\times10^{-3}$ kg, $Q_L=4.72\times10^{-7}$ m^3 s^{-1}, $u_G=1.5\times10^{-2}$ m s^{-1}, $k_d=8.82\times10^{-5}$ s^{-1}.

neously the kinetic parameters and k_d, the lowest value of the optimization criterion was obtained for k_d=0 and kinetic parameters equal those given in Table 1. Then, using $k_d=1.13\times10^{-4}$ s^{-1}, corresponding to the maximum value obtained in the airlift reactor, the concentration profiles were simulated showing only slight deactivation (Fig. 11). Only the MCC and CE profiles were slightly affected by deactivation at the end of the longest reactions. By conducting another optimization of the kinetic constants on eight experiments performed at T=353 K with a fixed value of $k_d=1.13\times10^{-4}$ s^{-1}, it was found that these constant values were very similar to those obtained without deactivation. Thus, deactivation cannot explain the different values of k_1^o and k_2^o in the airlift and batch reactors.

The second reason concerns the initial state of the catalyst. Considering the differences in the operating

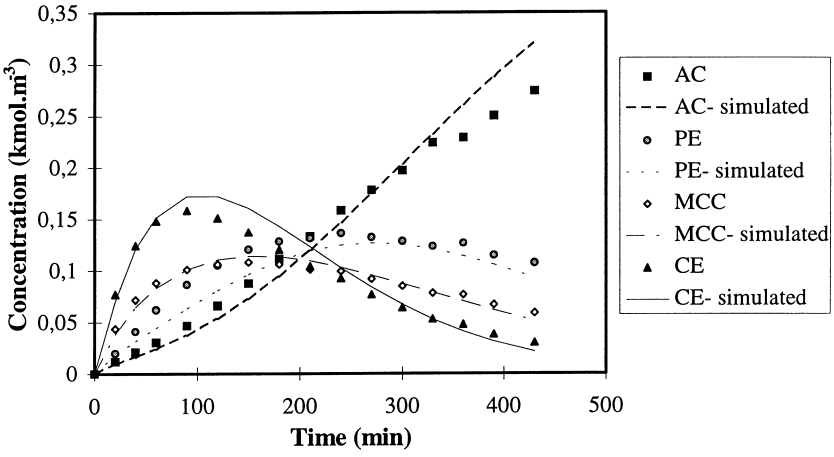

Fig. 10. Experimental and simulated concentration profiles versus time. $P_{H_2} = 2$ MPa, T=353 K, $C^o_{AC} = 0.475$ kmol m^{-3}, m_{cata}=5×10^{-3} kg, Q_L=4.72×10^{-7} m^3 s^{-1}, u_G=2.04×10^{-2} m s^{-1}, k_d=1.13×10^{-4} s^{-1}.

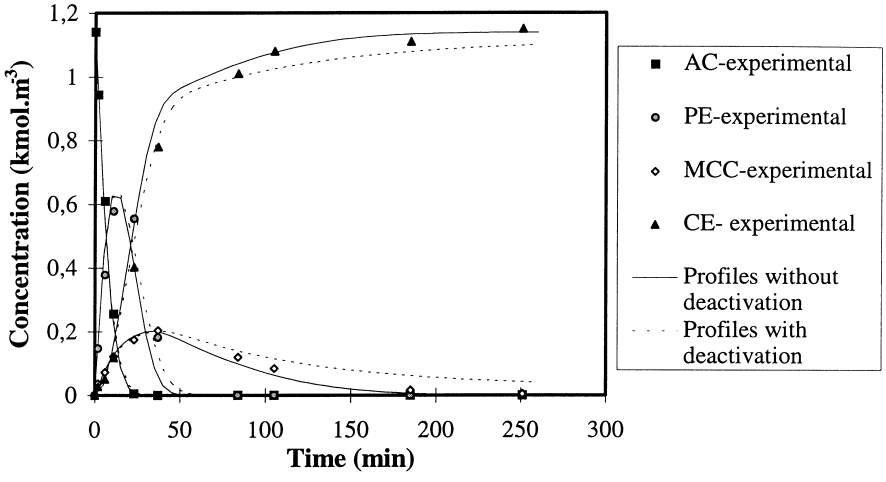

Fig. 11. Experimental and simulated concentration profiles versus time in semi-batch reactor with and without deactivation. $P_{H_2} = 2$ MPa, T=353 K, $C^o_{AC} = 1.14$ kmol m^{-3}, m_{cata}=5×10^{-4} kg, k_d=1.13×10^{-4} s^{-1}.

cycles of semi-batch and airlift reactors, it is possible that the state of the catalyst at the beginning of the reaction was not rigorously the same. Even if the catalyst pretreatment procedure (in cyclohexane during 1 h, under $P_{H_2} = 1.8$ MPa and T=368 K) was identical in both reactors, all the operating steps before the reaction might not be strictly reproduced. For example, the ratio m_{cata}/V_{liq} was 2.6 times higher in the semi-batch than in the airlift reactor. Moreover, due to different apparatus sizes, the time required to reach 368 K was much longer in the airlift reactor ($\approx 1\frac{1}{2}$ h) than in the semi-batch reactor (5–10 min). The time of contact between the catalyst and the solvent was not the same before the reaction. In order to evaluate the impact of the pretreatment procedure, two experiments were performed in the semi-batch reactor: one with a catalyst pretreated during 1 h at T=368 K and the other with a catalyst pretreated 15 min at T=353 K. Similar activities of the two catalysts were observed but the concentration profiles represented in Fig. 12 indicated a strong effect of pretreatment conditions on the selectivity. More

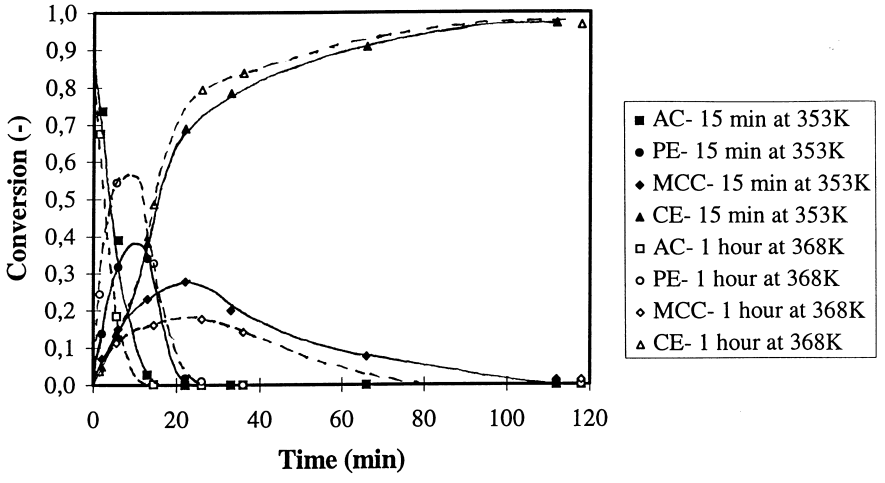

Fig. 12. Pretreatment effects on selectivities in semi-batch reactor. $P_{H_2} = 2\,MPa$, T=353 K, $C^{o}_{AC} = 0.624\,kmol\,m^{-3}$, $m_{cata}=5\times10^{-4}$ kg.

particularly, the PE and MCC profiles were strongly affected by a difference in catalyst pretreatment. This result could explain the unexpected selectivity obtained in the airlift reactor. The need of another optimization of the two kinetic constants for modeling the airlift performances is probably due to different initial state of the catalyst related to differences in the pretreatment procedures.

Secondly, the influence of the operating conditions on deactivation can be discussed considering k_d values obtained for each experiment (see Table 4). Deducing a general law for k_d as a function of operating parameters was not possible due to the restricted number of experiments but the following tendencies were observed, where the value of the deactivation constant k_d:

- increased with hydrogen flow rate,
- decreased with catalyst loading, and
- increased with the inlet concentration of acetophenone.

The increase with hydrogen flow rate is surprising while there is no significant hydrogen mass transfer limitation. Considering the high purity of hydrogen (Hydrogen U 99.995% Airgaz) used and its recycling, the hypothesis of poisoning by an impurity contained in the gas feed is highly improbable. The presence of a remaining impurity in the gas recycle pipes, pumps and condenser would be more probable. At high hydrogen flow rate, the recycling rate being higher, higher quantities of poison would be transferred per unit of time.

The variations of k_d with acetophenone inlet concentration and catalyst loading suggest the presence of an impurity in the liquid feed possibly being the reactant or the products of reaction themselves, progressively poisoning the catalyst. Even if this hypothesis is not sufficient to explain the variation of k_d with hydrogen flow rate, the observed tendencies could help in finding causes and mechanisms of deactivation.

6. Conclusion

An airlift reactor model was developed in the case of hydrogenation of acetophenone, a complex multistep reaction, including a first-order deactivation rate. This model provided a satisfying representation of all the experimental data, after readjustment of two kinetic rate constants and optimization of the deactivation parameter on each experiment. This modeling points out the complexities one has to face in order to work in a continuous reactor. Even if the kinetics of the reaction are well established and the hydrodynamics of the reactor well known, some additional phenomena due to the catalyst specificity such as deactivation or pretreatment effects can interfere and become predominant. In this case, kinetics should not be worked out in different reactors like batch

reactors easier to handle. The deactivation of the catalyst has to be studied in continuous reactors and, for this purpose, the slurry airlift reactor is well adapted but further work should be done in order to elucidate the causes and mechanisms of deactivation.

7. Notations

A	deactivation parameter (Nl min^{-1})
a	gas–liquid interfacial area, per volume of reactor (m^{-1})
C_i	concentration of i (kmol m^{-3})
C_i^o	concentration of i at the inlet of continuous reactors (kmol m^{-3})
C_s	solid concentration (wt%)
d_p	average particle diameter (m)
D	$= (1/K_{PE} + Q_{AC}[AC] + [PE] + Q_{MCC}[MCC] + Q_{CE}[CE])(1 + K_{H_2}He[H_2])$
D_i	molecular diffusivity of i (m^2 s^{-1})
error	relative error on Y_i^{exp}
He	Henry constant (Pa m^3 $kmol^{-1}$)
k_d	deactivation constant (s^{-1})
k_L	global liquid–solid mass transfer coefficient (m s^{-1})
k_i	rate constant of the reaction i (mol kg^{-1} s^{-1})
K_i	adsorption constant of i (m^3 $kmol^{-1}$)
m_{cata}	weight of catalyst (kg)
N	$= K_{H_2}P_{H_2} = K_{H_2}He[H_2]$
P	pressure (Pa)
Q_i	adsorption constants ratios K_i/K_{PE}
Q_L	liquid flow rate (m^3 s^{-1})
Q_{H_2}	instantaneous hydrogen flow rate consumed (Nl min^{-1})
r_i	intrinsic rate of reaction (kmol kg^{-1} s^{-1})
r_i^o	initial rate of reaction without deactivation (kmol kg^{-1} s^{-1})
t	time (s)
T	temperature (K)
u	velocity (m s^{-1})
V	volume (m^3)
Y_i^{cal}	calculated response value
Y_i^{exp}	experimental response value
Y_i^{max}	maximum experimental response value

Symbols

$[i]$	concentration of i (kmol m^{-3})

Subscripts

cata	catalyst
G	gas
H_2	hydrogen
l or L	liquid
r	reactor
S	solid
*	at saturation

Greek letters

ϵ	retention (dimensionless)
θ_{des}	fraction of deactivated sites (dimensionless)
ΔH_H	heat of adsorption of H_2 (kJ mol^{-1})

References

[1] L.K. Doraiswamy, M.M. Sharma, Heterogeneous reactions. Analysis, examples and reactor design, Fluid–Fluid–Solid Reactions, vol. 2, Wiley, New York, 1984.
[2] K.R. Westerterp, W.P.M. Van Swaaij, A.A.C.M. Beenackers, Chemical Reactor Design and Operation, Wiley, New York, 1984.
[3] J.B. Joshi, P.V. Shertukde, S.P. Godbole, Rev. Chem. Eng. 5(1)(2)(3)(4) (1988) 71–151.
[4] D.V. Mushenko, E.G. Lebedeva, V.P. Khimich, V.S. Chagina, N.S. Barinov, Zhur. Priklad. Khim. 39 (1966) 2766.
[5] D.V. Mushenko, E.G. Lebedeva, V.S. Chagina, V.P. Khimich, N.S. Barinov, Zhur. Priklad. Khim. 39 (1966) 2769.
[6] N.S. Barinov, D.V. Mushenko, E.G. Lebedeva, Zhur. Priklad. Khim. 42 (1969) 2398.
[7] N.S. Barinov, E.G. Lebedeva, D.V. Mushenko, Zhur. Priklad. Khim. 42 (1969) 2613.
[8] N.S. Barinov, D.V. Mushenko, Zhur. Priklad. Khim. 46 (1973) 940.
[9] N.S. Barinov, D.V. Mushenko, Izvest. Otdel. Khim. Nauk. 6 (1973) 507.
[10] P. Geneste, Y. Lozano, C.R. Acad. Sci. Paris, Ser. C 280 (1975) 1137.
[11] J. Masson, P. Cividino, J.M. Bonnier, P. Fouilloux, Heterogeneous Catalysis and Fine Chemicals II, vol. 59, 1991, p. 245.
[12] D.V. Mushenko, N.S. Barinov, E.G. Lebedeva, Zhur. Organ. Khim. 7 (1971) 314.
[13] G. Csomontanyi, M. Netta, M. Balmez, Revue Roumaine de Chimie 18 (1973) 1367.
[14] B.R. Serebryakov, N.A. Smirnova, V.G. Garbuzov, Azerb. Khim. Zh. 6 (1977) 135.
[15] F.B. Del Amo, Ingenieria Quimica (Madrid) 23 (1991) 115.
[16] L. Cerveny, Z. Dobrovolna, Z. Belohlav, P. Kluson, Collect. Czech. Chem. Commun. 61 (1996) 764.

[17] A.S. Ziyatdinov, V.V. Stepanenko, I.S. Chernykh, E.B. Leonova, V.N. Pisarenko, V.V. Kafarov, Zhur. Priklad. Khim. 61 (1988) 565.
[18] N.A. Smirnova, V.L. Adamyan, E.I. Edigavora, I.A. Likhushkin, Azerb. Khim. Zh. 4 (1987) 44.
[19] I. Bergault, These de Doctorat, Toulouse, France, 1997.
[20] R. Hibgie, Trans. AIChE 35 (1935) 365.
[21] P.V. Danckwerts, Ind. Eng. Chem. 43 (1951) 1460.
[22] C.R. Wilke, P. Chang, AIChE J. 1 (1955) 264.
[23] W.D. Deckwer, Bubble Column Reactors, Wiley, Chichester, UK, 1992.
[24] P. Weiland, U. Onken, Ger. Chem. Eng. 7 (1981) 374.
[25] L.S. Fan, S.J. Hwang, A. Matsuura, Chem. Eng. Sci. 39 (1984) 1677.
[26] L.S. Fan, Gas–Liquid–Solid Fluidization Engineering, Butterworths Series in Chemical Engineering, 1989.
[27] K. Koide, K. Horibe, H. Kawabata, S. Ito, J. Chem. Eng. Jpn. 18 (1985) 248.
[28] O. Levenspiel, Chemical Reaction Engineering, 2nd ed., Wiley, New York, 1972.
[29] G.F. Froment, K.B. Bischoff, Chemical Reactor Analysis and Design, Wiley, New York, 1979.